

EXPERIMENTS WITH LONG LIQUID COLUMNS UNDER MICROGRAVITY

I. Martínez¹ and A. Sanz²

¹Dept. Sistemas Oceánicos y Navales, E.T.S.I. Navales, Ciudad Universitaria, E-28040-Madrid
²Lamf/ETSIA, Laboratorio de Aerodinámica, E.T.S.I. Aeronáuticos, Ciudad Universitaria, E-28040-Madrid

ABSTRACT

This paper presents an updated analysis of the mechanical response of long liquid bridges during experiments carried out in Spacelab-D1 in 1985. The objectives of the experiment are revisited and a rigorous analysis of the data reduction process is given. Results on the measurement of residual accelerations imposed by the carrier, using the liquid column as transducer, are presented. A quick-look procedure to estimate the stability margins of a near-equilibrium shape, by just looking at the radial deformation at a quarter of its length and comparing it with theoretical equilibrium diagrams, is shown at work.

Keywords: capillarity, liquid bridge, microgravity, stability, g-jitter, floating zone, Spacelab.

1. INTRODUCTION

A liquid bridge spanning between two solid supports (as sketched in Fig. 1) represents a fluid interface configuration of high interest to both basic science and technology, the typical example of the latter being the molten bridge in the floating zone technique of crystal growth [1].

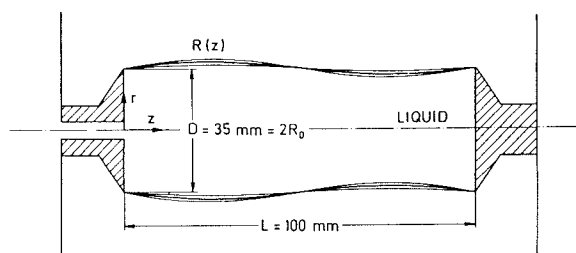


Fig. 1. Typical geometry of liquid columns in SL-D1. An equilibrium shape in the presence of residual axial acceleration, and the two bounds for small oscillations around equilibrium, are sketched.

For large, curved, fluid interfaces, the cylindrical liquid column has the simplest geometry except for the spherical one (drops and bubbles), but the difficulty in handling those isolated entities displaces the cylindrical liquid bridge to the foreground of interest. This explains why so many experiments with liquid bridges have been performed under microgravity since the pioneering demonstrations in Skylab in 1974.

The theoretical analysis of the mechanical behaviour of long axisymmetric liquid bridges anchored to the sharp edges of the supporting discs may be centered in the study of equilibrium shapes and their stability limits, frequency response and resonances, rotation of the bridge, and so on [2]. For instance, axisymmetric equilibrium shapes are characterised by the meridian curve (outer shape) $R=R(z)$ (bold letters refer to dimensional variables) as a function of the configuration and stimuli applied, namely: the radius of the supporting discs R_1 and R_2 (may not be equal), disc separation L , liquid volume V , residual acceleration g in the axial direction of the column, and solid-body rotation speed Ω . Introducing non-dimensional variables: $z \equiv z/R_0$, $R \equiv R/R_0$, $H \equiv (R_2 - R_1)/(R_2 + R_1)$, $\Lambda \equiv L/(R_2 + R_1)$, $V \equiv V/R_0^3$, $B \equiv \Delta\rho g R_0^2/\sigma$, $W \equiv \Delta\rho \Omega R_0^3/\sigma$, with $R_0 \equiv (R_2 + R_1)/2$, where B and W are the traditional Bond and Weber numbers, and assuming the set of parameters (H, Λ, V, B, W) given, the outer shape, $R=R(z)$ can be computed by numerical integration of the second order differential (Young-Laplace) equation:

$$C(z) - B.z + \frac{W}{2} R^2(z) + P = 0 \quad (1)$$

where $C(z)$ is the local mean curvature at a point in the shape:

$$C(z) \equiv \frac{R_{zz}}{(1 + R_z^2)^{3/2}} - \frac{1}{R(1 + R_z^2)^{1/2}} \quad (2)$$

and P is the non-dimensional gauge pressure at the origin, an implicit constant that must be also computed from the boundary conditions: $R|_{z=0} = 1 - H$, $R|_{z=2\Lambda} = 1 + H$, and $\pi R^2 dz = V$.

The integration can be performed by the shooting method (the one used here), or by finite differences, and in the case $B=W=0$ it can be even expressed analytically in terms of elliptic integrals. The goodness of a given meridian curve $R=R(z, H, \Lambda, V, B, W)$ as an equilibrium shape can be measured by the deviation ϵ , defined as:

$$\epsilon \equiv \int_0^{2\Lambda} [C - B.z + \frac{W}{2} R^2 + P]^2 dz \quad (3)$$

The stability limit when varying a parameter is found by looking at the zeroing of the jacobian of the transformation from the two guessed parameters used to start the shooting (unknown initial slope and unknown P in Eqn. (1)) to the two target parameters H and V ; Λ , B and W are known. With the experiments of SL-D1 in mind, Fig. 2 has been prepared following those steps; they present, for shapes $R=R(z, H, \Lambda, V, B, W)$ with $H=W=0$, diagrams of a characteristic point in the shape (the radius at 1/4 of the length) and the stability limits in several drawing projections. From another point of view, the radius at 1/4 would correspond to the radius at 3/4 if the direction of the residual acceleration was reversed, and this is why one may talk exclusively of 1/4-values letting B have negative values also.

These computations are tedious, and analytical expressions are most wellcomed. In this respect, it is worth pointing out a rather simple approximation to the limit curve in Fig. 2b (for $V=V_{cy}=2\pi\Lambda$): $R_{1/4} = [1 \pm (4/3)(1 - \Lambda/\pi)^{1/2}]^{1/2}$.

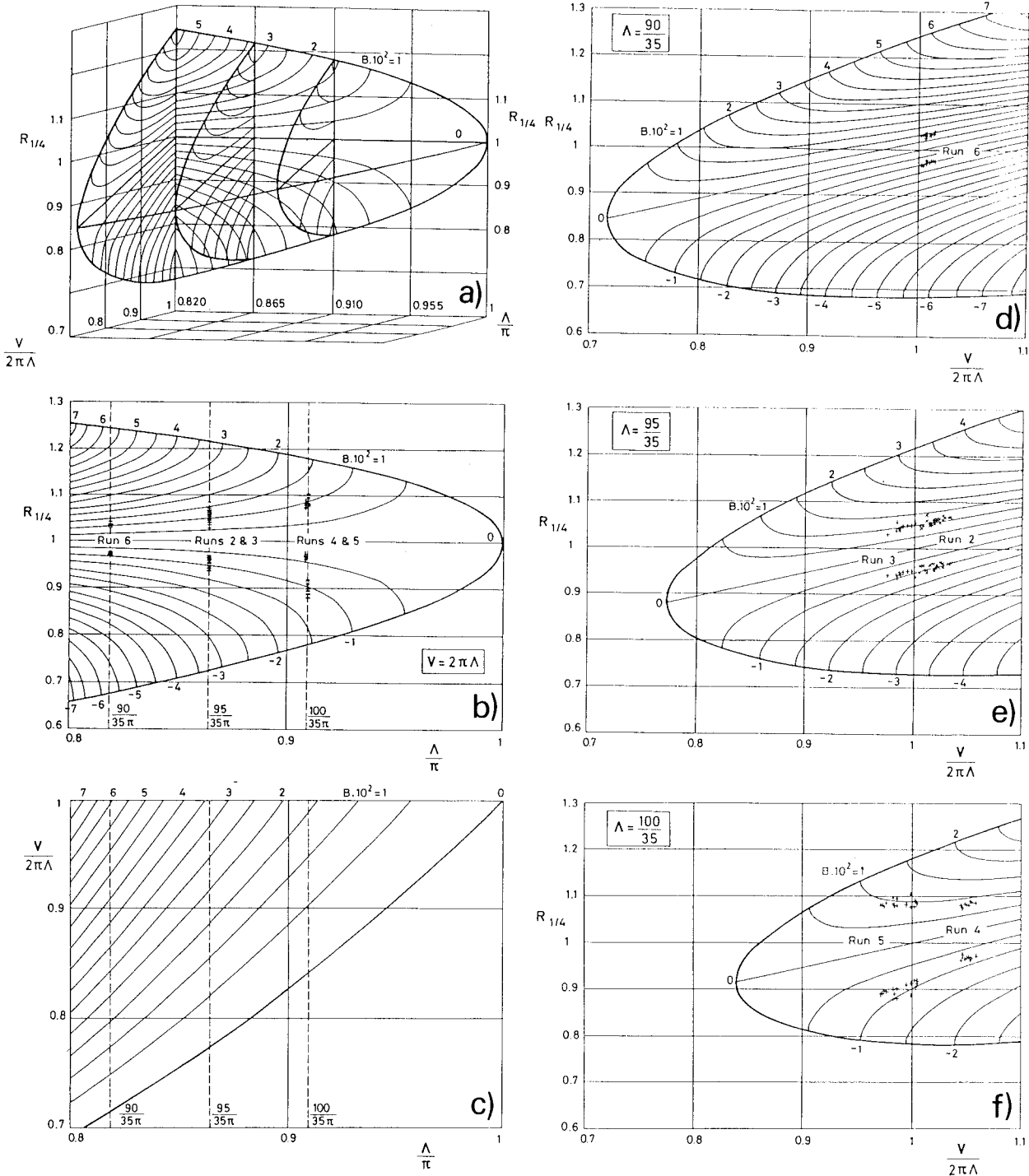


Fig. 2. a) Perspective of the theoretical radius at 1/4 of the length $R_{1/4}(\Lambda, V, B)$ as a function of the reduced slenderness Λ/π , reduced volume V/V_{cyl} and Bond number B . b) Cut by $V=V_{cyl}$ plane. c) Projection from above. d) Cut by $\Lambda=90/35$ plane. e) Cut by $\Lambda=95/35$ plane. f) Cut by $\Lambda=100/35$ plane.

However, all theories encompass some hypotheses and simplifications that must be checked if they are applicable or not, and in practice, unthought effects always appear. Thus, the general purpose of these experiments with liquid bridges (aplicable to many other problems) may be stated as follows: 1. To check that the response of the system to the applied stimuli is as predicted by theory; to this purpose, clear-cut check points (f.i. minimum volume of liquid for a bridge), with well controlled applied stimuli (precision control of disc separation, rotation and vibration) and little sensitivity to uncontrolled forces (f.i. working temperature), are

proposed for measurement. 2. To check the assumed hypothesis; when the response of the system is not as expected, the consistency of the theoretical development must be reviewed, and thence the applicability of the hypothesis introduced to simplify the analysis or model the system. 3. To see if new phenomena appear, and to quantify them; for instance, if a theory to account for the effect of the residual acceleration is available, and in this case it is, the experiment allows to estimate the actual value: for the experiment in SL-D1 a value of about $70 \mu g_0$, that is $7.10^{-5} \text{ m.s}^{-2}$, was obtained [3]).

In order to give a more structured idea of the several available theoretical models, the instantaneous states of a liquid bridge can be classified in the three following types:

1. Equilibrium states.

This is the simplest case, and if only mechanical forces are acting, shapes can be easily computed as explained above. An experiment on equilibrium shapes consists of procuring well-defined stimuli (H,Λ,V,B,W), recording the actual shape, extracting from that shape the corresponding theoretical values of the set (H,Λ,V,B,W), comparing both sets of parameters, and, after the uncertainties due to experimental error been accounted for, trying to explain the differences found.

2. Steady and periodic states.

Here, the time variable can be taken out of the problem because it does not appear (steady states) or because it enters as a separate harmonic term (periodic states) that modulates in a simple manner the spatial response (the period is well defined) Typical problems in this field are the periodic oscillations of the column when one (or both) of the end supports is forced to oscillate axially, and the steady state reached when one of the discs is forced to rotate at a constant rate (or both, at equal or different speeds). Besides the forcing parameter, other degrees of freedom appear on these problems (as the transport coefficients: viscosities of working liquid and outer fluid). In these cases, besides the outer shape of the bridge, the relative motion inside the fluids is also of great interest. Steady state theories are less developed, and a lot remains to be done (f.i. how is the flow structure in a counter-rotating liquid column?). Notwithstanding the fact that the dimension of the problem has grown (still confining oneself to axisymmetric motions), a major experimental handicap appears also: the diagnosis of the motion inside the liquid column is very difficult because its curved interface (particularly if it is not nearly-cylindrical) renders the optical diagnosis cumbersome. Small tracer particles added to the liquid are normally used for qualitative visualization (as was done in these experiments) making them visible with a meridian light sheet, but quantitative analysis has always somehow resisted.

3. Transient states.

In this case, time is the most important variable. Besides all the transient problems encountered during the formation of a long liquid column (emerging capillary flows, detachment, spreading, anchoring, filling liquid, separating the discs, removing liquid, etc), some transient problems with already established cylindrical liquid columns are of interest. Particular attention has been paid to the evolution during the breakage of the column beyond the stability limit [4], to the onset of convection by spinning one or both discs [5], and to the cylindrical liquid injection (injection and separation to keep a cylindrical volume) [6]. Transient problems require such a strict control of the initial conditions, and demand such a comprehensive diagnosis (with variables changing their ranges and relative importance through the evolution) that no attempt to have detailed quantitative measurements has yet been exercised in a microgravity platform.

During experiment execution in SL-D1 the ambient mechanical noise (so called g-jitter) forced the liquid to be in a permanent state of motion, although fortunately of small amplitude. Instead of just concluding that Spacelab was found to be a noisy environment not suitable to delicate experiments with liquid bridges at equilibrium, a deep analysis of the consequences has been performed, trying to extract the maximum of information from the available (rare, unique and costly) data.

2. UNCERTAINTY IN DATA REDUCTION

A common feature to data reduction in all cases is to investigate the uncertainty threshold that separates the region of values in agreement (those that, because of the imperfections in measurement and data analysis, are judged as acceptable) from the region of values in disagreement (those that require further explanation in terms of uncontrolled perturbances, failure of the measurement process, etc).

A set of well defined configuration and stimuli parameters are applied; in this case (H, Λ, V and W), and besides, other uncontrolled stimuli are acting upon, some modifying the equilibrium (f.i., a constant axial acceleration, that yields an unknown B value) and others forcing a dynamical evolution (periodic or not) that in this case is small and thought to make the equilibrium analysis (detailed below) still meaningful.

Equation (1) is still the correct boundary condition for the pressure jump across the interface (normal stress for an inviscid flow), but now P is no longer a constant, because the equation of motion (axial momentum equation) is no longer $0 = -dp/dz + \rho g$, but $\rho[\partial w/\partial t + u\partial w/\partial r + w\partial w/\partial z] = -dp/dz + \rho g$, where p is the pressure field, and w and u the axial and radial components of the velocity field. One may thence still think of a constant P with an extended form of Eqn. (1), namely:

$$C(z) - B.z + \frac{W}{2} R^2(z) + P + K(z) = 0 \tag{4}$$

(where K(z) is the appropriate kinetic term) as the exact equation to be verified at each point of each instantaneous shape. To compute K(z), the exact velocity field must be known. A scale analysis gives:

$$|K(z)| \approx \frac{\int \rho w_t dz}{\sigma / L} = \frac{\iint \rho (-2R_{tt} dz) dz}{\sigma / L} = \frac{\rho (-\frac{2\Delta R_L}{T^2}) L}{\sigma / L} \tag{5}$$

or, in nondimensional units, $|K(z)| = 2\Lambda^3 \Delta R / T^2$, with ΔR being the amplitude of the radial oscillations and T the period.

With the assumption that, for near-critical slendernesses and very low frequencies, the natural oscillations correspond to a shape deformation given by:

$$R^2(z) = 1 + 2B(z-\Lambda-\lambda \frac{\sin(z-\Lambda)}{\sin \Lambda}) + (\frac{V}{2\pi\Lambda} - 1)(1 + \cos \frac{\pi(z-\Lambda)}{\Lambda}) + \Delta R \sin \frac{\pi z}{\Lambda} \sin \frac{2\pi t}{T} \tag{6}$$

(which is based on Eqn. 3 of [4]), one may compute in full K(z), because for linear dynamics it may be estimated just from shape evolution. From the equations of motion for the linear one-dimensional slice model [4], $\partial K/\partial z = \partial w/\partial t$ and $\partial w/\partial z = -2\partial R/\partial t$, one obtains:

$$K(z) = \frac{8\pi\Lambda^2\Delta R}{T^2} (\frac{z}{\Lambda} - 1 - \frac{1}{\pi} \sin \frac{\pi z}{\Lambda}) \tag{7}$$

Taking $|K(z)| = 8\pi\Lambda^2\Delta R/T^2$, with $\Lambda=3$, $\Delta R=0,01$ and $T=40$, gives $|K(z)|=0,01$. The other terms in Eqn. (4) are $|C(z)|=1$, $|P|=1$ and $|B.z|=0,03$ (it is assumed $W=0$).

In SL-D1, photographs were taken of nearly-cylindrical liquid columns subjected to an unknown microgravity level corresponding to an static Bond number of order 10^{-2} , superposed to an unknown dynamic contribution with a similar weight ($K=0,01$), and the column shape is digitized with an uncertainty in the radius also of 10^{-2} . Is it possible to extract more information from this noise and get f.i. a precise figure for the Bond number?

If the uncertainty in R(z), K(z) and B were all of the same type, nothing more could be resolved; but if one assumes that the discretization uncertainty in R(z) corresponds to white random noise, and one knows that the uncertainty in K(z) is modulated in time with a known period (about 20 s for Run 2, 28 s for Run 3, 32 s for Run 4, 44s for Run 5 and 21 s for Run 6, as shown below) whereas the uncertainty in B is stationary with time, much more information can be extracted.

But before this is done, it seems appropriate to look in more detail to the data gathering process, because one may accept the uncertainty due to kinetic effects in exchange for the simplification of not having to study the dynamic response of the system, but why one should accept a 1% uncertainty in the digitization of the liquid outer shape?, cannot it be done much more precisely?

At first sight, all the stimuli being mechanic, one might hope to reach "mechanical precision", say with relative uncertainties below

10^{-4} , but a more careful look shows how different it is in reality. To begin with, a high precision apparatus (the FPM) was developed to sustain these experiments in Spacelab. The machining of the support discs and the axial displacement of one disc met the above tolerances (in size, concentricity, parallelism, offset, etc).

The problem of knowing before-hand the liquid volume, a highly important parameter, can be circumvented, because the estimated uncertainty when computing the volume of an axisymmetric body after the image of its contour can be very low indeed, at least in principle. Related to this point is how to measure the outer shape of the column. To this purpose, both a 16-mm film and a video camera have been used to record images of the bridge, and, although this is a straightforward step on ground, it has been troublesome in these early flights, with partial failures in film transport and video recording.

The visualization of the liquid bridge in the FPM is also much worse than in normal Plateau-tank work on ground, as may be compared from Fig. 3, due to the many compromises adopted (volume allocation in the FPM was frozen in 1977, the experimenters have restricted access to the FPM during ground trials, etc). Add it to the fact that a conical view of a 100 mm object is taken from a 400 mm distance, and it becomes apparent that, even if everything else worked perfectly, the reconstruction of the outer shape from the images would not be as simple and accurate as thought.

The objective of the digitization process is to extract from every image the profile of column thicknesses and the profile of lateral shifts from the viewing projection, because, although actual shapes are not strictly axisymmetric, a slice model is assumed in which the three-dimensional liquid column is approximated by a series of circular slices (with the diameter seen in the viewing projection) slightly displaced off-axis.

From several tests, the uncertainty introduced by the operator in the digitizing process was estimated to be about $\pm 1\%$ relative to the undisturbed radius; this is not a high figure of merit, because one is

interested in small deviations from the cylindrical shape and the average error relative to the mean deviation may reach 20% or 30%. The operator adjust the outlines in the digitizing tablet so as to share a common origin and common axis (by sight). It was found, however, that the slenderness (L/D) of the liquid column computed from the digitization consistently departed some 3% from the nominal scheduled one (known to be correct from the housekeeping data of the FPM); because this is beyond the operator uncertainty, and based on the consistent bias, this was attributed to optical distortion in the magnifying projector, and the FPM data was granted full confidence and used to stretch the digitized shape to force it to have that slenderness (losing redundancy in the data).

All points in the digitized shape had the same uncertainty, including the four corners that define the limits of the column. The aim was to produce two normalized curves: the thickness profile and the lateral-shift profile, so that a normalization was needed to force that all column thickness start and end with unit value (the discs radius), and all lateral-shifts start and end at zero (the discs were not moving laterally). To this purpose, several procedures were tried: first smooth the data with a standard curve smoothing routine and then adjust the diameters and length; first adjust and then smooth with a routine that conserve the end points, etc. All procedures tried seemed good (the fact is that in this case the corrections are very minute, but this is a delicate problem in general), and the choice finally adopted was to first get the raw profiles of thicknesses and lateral-shifts, then smooth those profiles with a few-terms Fourier approximation, and last, to force the adjustment at the ends.

Once the basic uncertainty introduced by the operator ($\pm 1\%$) taken into account, the two most important parameters involved in the data reduction process are: 1) how many points, N_p , must be digitized for each shape, and 2) how many terms, N_f , in the Fourier approximation must be used to clean the shape from all the digitization noise. These are key-points in any digitization process, be it manual or automated, so that a special effort was devoted to better understand them.

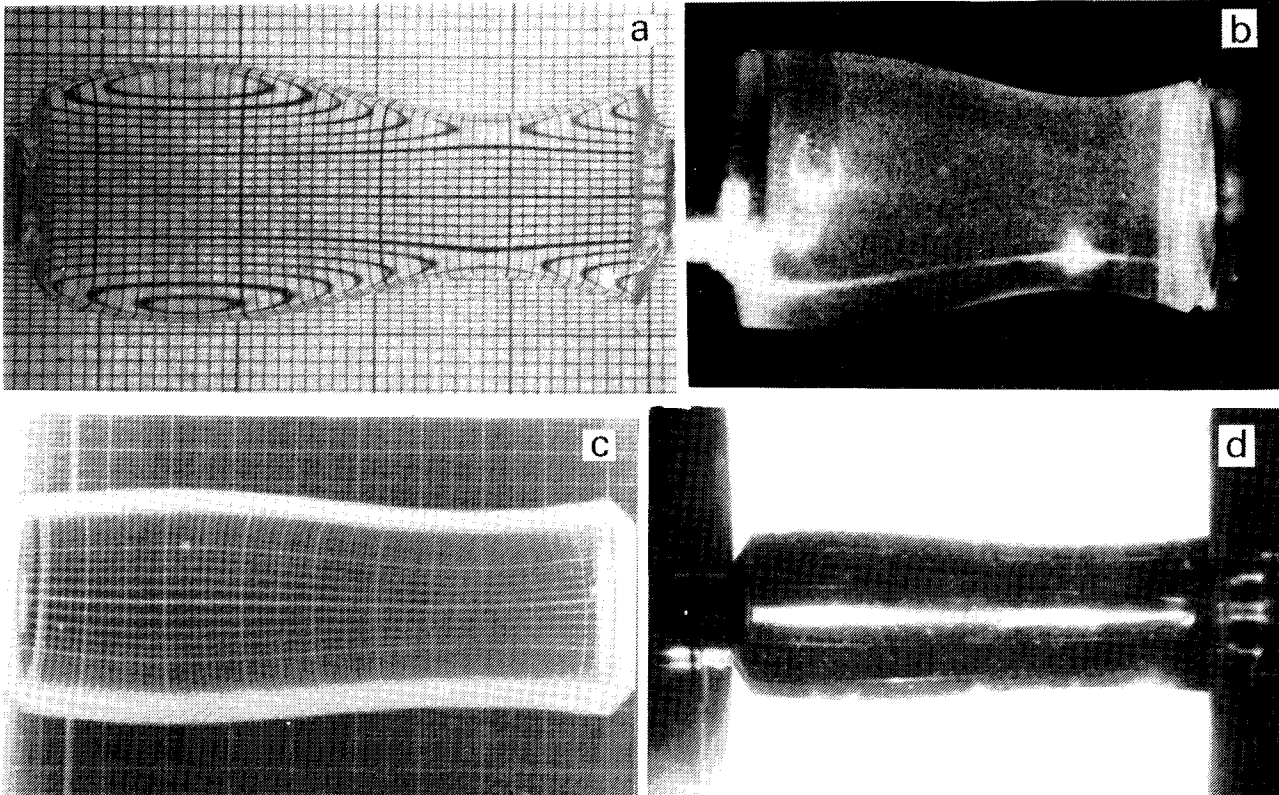


Fig. 3. Comparison of image quality. a) Plateau tank on ground: $2R=30$ mm and $L=83$ mm. b) Spacelab-1 (1983): $2R_1=50$ mm, $2R_2=60$ mm and $L=95$ mm. c) TEXUS-18 (1988): $2R=30$ mm and $L=80$ mm. d) Spacelab-D1 (1985): $2R=35$ mm and $L=100$ mm.

To this purpose, five relevant equilibrium shapes (see Fig. 4) were numerically generated (with the shooting method) with a high precision at its equally-spaced $N_p=100$ points (what means that the uncertainty ϵ (Eqn. (3)) is below 10^{-5} , well outside the range of concern here. Thence, the same random deformation (of amplitude $\pm 1\%$ of the radius) is added to the radial coordinates of the five shapes, and the normalization described above applied. It is reckoned that the addition of a white-noise random deformation at each point may not be adequate to represent the human operator error, because humans tend to correlate nearby errors, have time-memory and act on goals, but it may help anyway. For the Fourier transform, the function $R(z)$ is extended antisymmetrically, and thus, due to its continuity (the effect of noise at the end-points is small) and to its continuous derivative due to the antisymmetric replication, the coefficients will decay with n^{-3} [7].

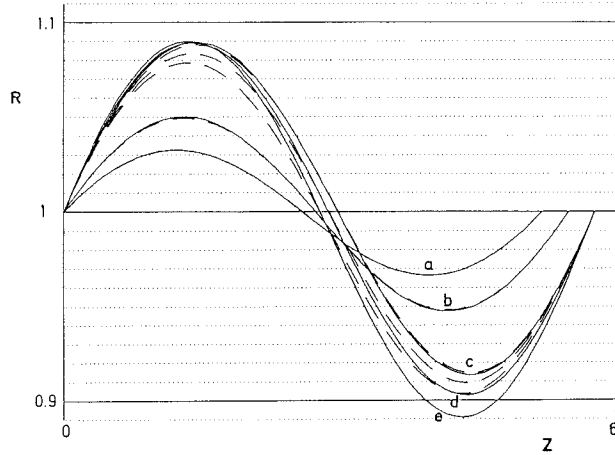


Fig. 4. Five test-shapes $R=R(z)$ chosen to analyze the effect of the digitization noise by computer simulation. The defining set of parameters (λ, V, B) are as follows: a) $(90/35, 2\pi 90/35, 0.010)$, b) $(95/35, 2\pi 95/35, 0.010)$, c) $(100/35, 2\pi 100/35, 0.010)$, d) $(100/35, 2\pi 100/35 \times 0.99, 0.010)$, e) $(100/35, 2\pi 100/35 \times 1.01, 0.010)$. Linear approximations using Eqn. (6) are plotted dash, for comparison.

Figure 5 shows a log-log plot of the Fourier coefficients for the 5 test-shapes, both exact and when distorted with a white noise of amplitude 0,02 peak-to-peak. From that one may observe the following facts: 1) the decay with the n^{-3} law for the exact shapes, 2) the lack of decay when white noise is applied, 3) the coincidence of the tail coefficients for all noisy shapes because the noise was the same, 4) the reduction from input noise level (0,02) to modulus of

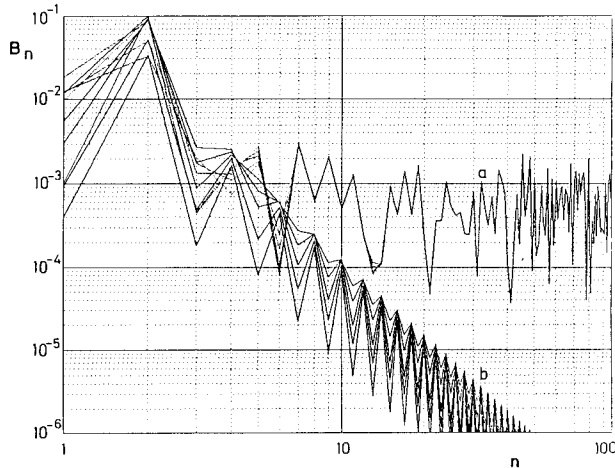


Fig. 5. Fourier spectrum of the test-shapes of Fig. 4, with (a) and without (b) an added white noise of $\pm 1\%$ radial amplitude. A sine development is used, with 100 terms (because the shapes were represented at 100 test-points), B_n being the amplitude of the n th term. The random noise at each point is the same for all test-shapes.

tail coefficients (≈ 0.001) which is proportional to $N_p^{-1/2}$. Notice also that the first coefficient gives an idea of the departure of the shape from the cylindrical volume, and that the second one is proportional to the residual gravity level, which is the cause of the largest departure from the cylindrical shape.

From Fig. 5, it becomes clear that there is no point in retaining beyond the sixth term in the series expansion (this value might have been found from the decay law for the coefficients and the noise level), implying that an uncertainty of 10^{-3} must be assumed from the digitization process (and not $2 \cdot 10^{-2}$ that was the input noise), and that the number of points to be digitized N_p may be reduced from 100 to 25 with an uncertainty growth from 10^{-3} to $2 \cdot 10^{-3}$. Actually, 52 points per shape (26 for each side) were digitized because it happened to better suit the available grid paper.

3. DATA ANALYSIS

A first goal of this analysis is to compare the sequence of non-axisymmetric and unsteady shapes digitized from SL-D1, with the equilibrium ones predicted by theory. To get rid of the unsteadiness due to g-jitter, the assumption is made that equilibrium shapes can be extracted after averaging actual shapes over one cycle of the first natural frequency of the liquid column, as shown in Fig. 6 for a column subjected to bare g-jitter and for a column with an oscillation on top of the background g-jitter. This hypothesis, even with the assumption of linear deformations in an inviscid fluid, has several deficiencies: first, the mean shape is not an equilibrium shape because there are fluid velocities and they would modify the pressure field; second, only the effect of the first natural frequency is subtracted, but for low speeds these effect should be small and can be delimited as done before.

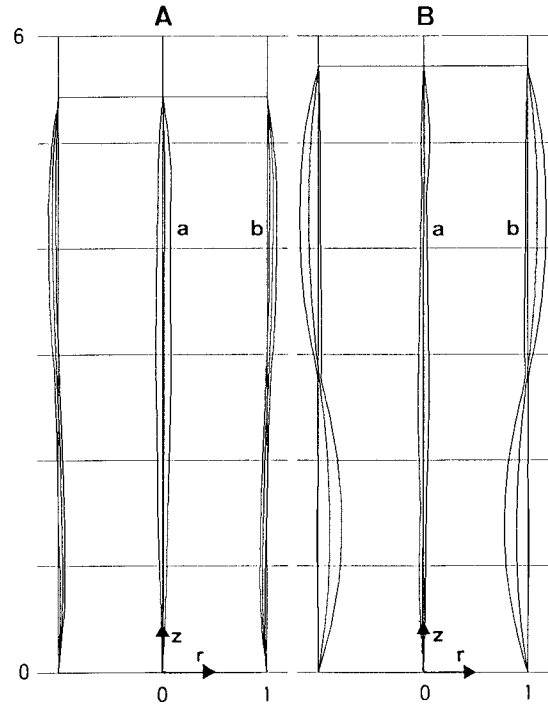


Fig. 6. A) Envelope of traces of 100 consecutive shapes shot at 2 s interval, of a 95 mm long column subjected to the bare effect of ambient g-jitter. B) Envelope of traces of 10 consecutive shapes shot at 2 s interval, of a 100 mm long column with a large oscillation (one half-period shown) superposed to the ambient g-jitter: a) Lateral shifts; from them, an averaged equilibrium shape (middle curve) is assumed. b) Meridian thickness profiles.

Figure 7 gives, in a strip-chart format, an overview of the digitized data from SL-D1: the time series of disc separation L , the time series of the Fourier coefficients B_n of pseudo-equilibrium shapes, and the corresponding Bond number for these shapes, computed as

said below, are shown. The aim of this plot is, besides giving the compound experiment sequence, to show how steady the averaged shapes are, how constant the Bond number is (≈ 0.01), a quick-look of volume variations (represented by B_1 , as explained below) and $R_{1/4}$ -values (B_2); B_3 , B_4 , B_5 and B_6 are shown to be negligible.

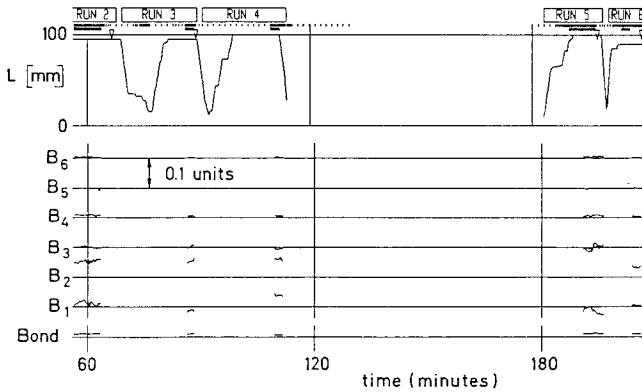


Fig. 7. Column length L (in mm) versus time (in minutes after SL-D1 time MET 06/00:00:00 [3]). Strip chart of the six Fourier coefficients B_n of the thickness profile and the corresponding Bond number of the averaged pseudo-equilibrium shapes. Below each Run label, the SL-D1 picture budget and the fraction digitized are shown, as well as the event of column breakage (∇).

From the pseudo equilibrium shapes computed from the experiments, the objective is to find the set of parameters (H, Λ, V, B, W) for comparison with the imposed set. This possibility is based on the fact that, except for singular cases (like the cylindrical shape in some instances, which, on the other hand are trivially simple), there is a biunivocal correspondence between shapes and sets of parameters.

Due to the adjustment forced on the digitized shapes, H and Λ are already accounted for, and, if one restricts the analysis to cases with $W=0$, the problem reduces to compute V and B from the pseudo-equilibrium shapes.

The volume, which is not an equilibrium property and can therefore be measured for unsteady shapes also, is computed from the thickness profile by Simpson's rule, with a relative uncertainty related to that of the shape by $\delta V \approx 2\pi \delta R / N_p^{1/2}$, what means that for a shape with an accuracy of $\pm 1\%$ and $N_p=52$, the uncertainty in volume is nearly the same: $\pm 1\%$. This applies to volume computation from just one shape; if one is certain that for a sequence of shapes the volume was maintained, averaging in time would further reduce that value; f.i. for a 100 frame sequence the volume uncertainty would be as low as $\pm 0.1\%$; there is no point to go any further (were it be possible), because the experimental data does not support the assumption of constant volume during such a long period (several minutes), even during processes that were nominally at constant volume, as shown later.

The relation between volume and Fourier coefficients in the $R(z)$ expansion:

$$R(z) = 1 + \sum_{n=1}^{\infty} B_n \sin \frac{\pi n z}{2\Lambda} \quad (8)$$

is as follows:

$$V = \pi \int_0^{2\Lambda} R^2 dz = 2\pi\Lambda \left[1 + \frac{4}{\pi} \sum_{n=1}^{\infty} \frac{B_n}{n} \right]_{\text{for } n \text{ odd}} + \frac{1}{2} \sum_{n=1}^{\infty} B_n^2 \quad (9)$$

what means that, to a first approximation, $B_1 \approx [V/(2\pi\Lambda) - 1]\pi/4$ measures the volume difference to the cylindrical one. From the time series in Fig. 7 one concludes that volume deviations are within the expected digitization uncertainty ($\pm 1\%$) except for the case of Run 4 where some other explanation, not yet found, must justify a 5% excess in volume.

On the other hand, the Bond number, introduced to measure the zero-frequency component of the residual axial acceleration, can only be found from equilibrium shapes, for which it can be computed by several methods:

1. By means of Eqn. (1), by linear regression of the points $P-B.z=-C(z)$ obtained when the pseudo-equilibrium shape is introduced in Eqn. (2). This is a second order differential procedure, and, although noise growth is effectively reduced with the Fourier expansion described above, it gives uncertainties in B up to 50%, according to the computer simulation.

2. By means of the theoretical shape $R=R(z, H, \Lambda, V, B, W)$, minimizing the distance S from the experimental shape $R_i(z_i)$ to the theoretical one $R(z, B)$ (at given H, Λ, V and W). This is achieved by solving the implicit equation:

$$\frac{\partial S}{\partial B} = 0 \quad \text{with} \quad S = \sum_{i=1}^n [R_i(z_i) - R(z_i, B)]^2 \quad (10)$$

If the linear approximation of Eqn. (6) is used (what is very accurate for shape departures from the cylinder less than 5%), Eqn. (10) can be solved explicitly, although in this case, it is better to define S as:

$$S = \sum [R_i^2(z_i) - 1 - 2B(z_i - \Lambda - \frac{\sin(z_i - \Lambda)}{\sin \Lambda})]^2 = \text{minimum} \quad (11)$$

The Bond number obtained from Eqn. (10) has been presented in Fig. 7 for each pseudo-equilibrium shape. It is remarkable to notice that B is practically uniform over three hours (two Shuttle orbits), and from its value $B=0,010$ a residual acceleration in the direction of the column axis of $g = \sigma B / (\rho R^2) = 0,7 \cdot 10^{-3} \text{ m.s}^{-1} = 70 \mu g_0$ is deduced. More precisely, $B=0,010$ along Runs 2, 3, 5 and 6, but $B=0,008$ along Run 4, and the constancy of B is so neat that one is inclined to extract information and perhaps ascribe it to the fact that Run 4 is also characterized by a volume departure from the cylindrical one (as seen from B_1 in Fig. 7); but adding the volume term of Eqn (6) to Eqn. (11) does not change the results.

Similarly to the relationship between B_1 and the volume V , there is a correspondence between B_2 and the Bond number, which can be found by Fourier expansion of $R(z, B)$ from Eqn. (6) in the form of Eqn. (8), obtaining:

$$B_n = \frac{-2B}{\frac{\pi \pi [1 - (\frac{n\pi}{2\Lambda})^2]}{2\Lambda}} \quad \text{for } n \text{ even} \quad (12)$$

being $B_2 = B/(\pi/\Lambda - \pi^3/\Lambda^3)$ the leading term.

3. By just locating the radius at 1/4 of the column length in the equilibrium diagrams shown in Fig. 2. Actually, because it does not add any difficulty and may be of help, both the radius at 1/4 and at 3/4 of the length are used. Results by this method are similar to the previous ones and now the procedure is straightforward. One may realise the importance of the effect of volume departure from the cylinder by looking at Run 4 points in $R_{1/4}$ vs Λ/π diagram in Fig. 2, where it might seem that Bond number values less than $B_1 0^2 = 0.5$ were achieved, and then finding the answer in the $R_{1/4}$ vs $V/(2\pi\Lambda)$ diagram, where a value of about $B=0.008$ can be seen.

The precedent data analysis was concerned with equilibrium shapes. Another goal of the present analysis is to look at the frequency response of the column, deduced from the photographs, both when forced at a given frequency (assumed unknown, although the settings were recorded), and when freely oscillating because an initial non-equilibrium condition.

Images were taken in the SL-D1 experiment at 2 seconds interval, what means a sampling rate of 0.5 Hz and consequently a bandwidth from 0 to 0.25 Hz (Nyquist criterion). The expected natural frequencies for the first axial mode were [15] about 0.11, 0.09 and 0.07 Hz for cylindrical liquid columns of $L/D=90/35$, $95/35$ and $100/35$, respectively (see [8] for an updated review). Besides, a liquid column of $L/D=95/35$ was forced to oscillate by displacing harmonically one of the support discs with an amplitude of 0.93 mm peak-to-peak at frequencies of 0.10, 0.30, 0.70, 1.10 and 1.60 Hz

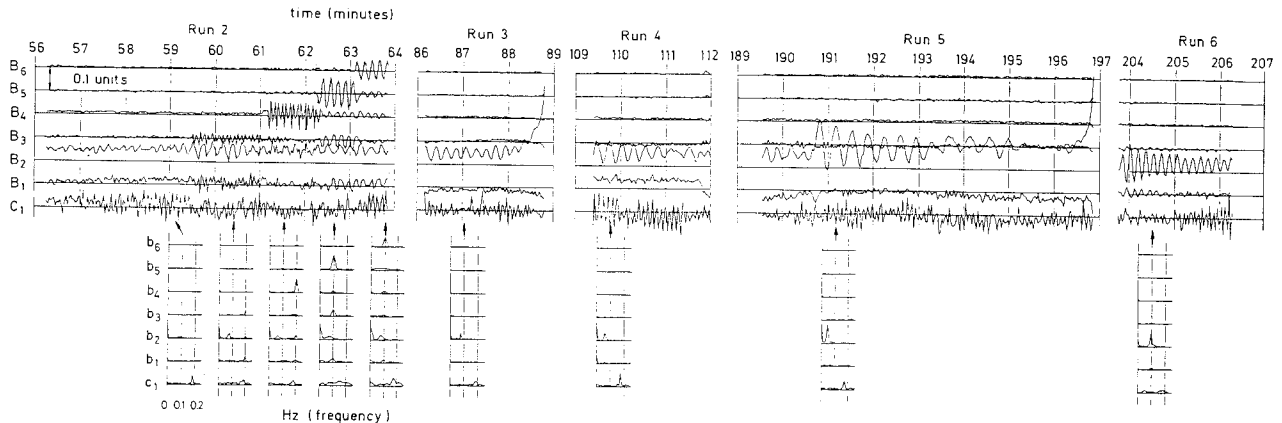


Fig. 8. Time series of the six Fourier coefficients B_n used to approximate each instantaneous shape thickness as the first Fourier coefficient C_1 of axial deviations. The temporal spectrum b_n and c_1 of these coefficients are also shown for selected periods of time (the complete Fourier expansion in sines and cosines is used). For Run 2, 228 frames are digitized, and the periods (in frame number) selected for the spectrum are 30-90, 100-145, 148-178, 185-205 and 205-225. For Run 3, 80 frames, and the period is 0-59. For Run 4, 79 frames, and the period is 0-49. For Run 5, 220 frames, and the period is 38-78. For Run 6, 77 frames, and the period is 1-43.

(roughly corresponding to the first 5 natural frequencies at that slenderness) during at least one minute each. The response of the liquid column is shown in Fig. 8 in terms of the time series of the six Fourier coefficients B_n used to approximate each instantaneous shape thickness, as well as the first Fourier coefficient C_1 (half a period of a sine) of axial deviations (C-mode). The temporal spectrum of these coefficients are also shown in Fig. 8 for selected periods of time. Run number 1 is not analysed here because the operator there could not manage to keep a cylindrical volume, as explained in [3].

Lateral oscillations were theoretically studied in [9] and result compare well for resonance frequencies deduced from Fig. 8, which correspond to a period of about 5 seconds.

One can see in Fig. 8 the effect of forced oscillations performed in Run 2, in perfect synchronism with the housekeeping data from the FPM. Although forcing frequencies were 0.1 Hz, 0.3 Hz, 0.7 Hz, 1.1 Hz and 1.6 Hz, due to the stroboscopic effect of shooting a picture every two seconds (0.5 Hz), only the combined frequencies 0.1 Hz, 0.2 Hz, 0.2 Hz, 0.1 Hz and 0.1 Hz are seen in the Fourier coefficients B_n and more explicitly in their temporal spectra b_n (mind that the first forcing frequency left a negligible fingerprint). In all Runs, the first natural frequency is seen in b_2 , being excited by the background g-jitter except for Run 5, where an abrupt stop in disc separation forced a step response. The natural frequency for lateral shifts can be seen in the spectrum of c_1 . Volume departure from the cylinder is visualized by B_1 , as said above.

4. CONCLUSIONS

The objectives pursued and results achieved from these SL-D1 experiments can be summarized as follows:

To build large and slender liquid bridges ($L=100$ mm). It was done successfully on several instances, in a controlled manner not achieved before (the liquid filling process, the wetting and anchoring at the edges, etc., were mastered).

To approach the Plateau limit ($\Lambda/\pi=1$). Trials were performed at an slenderness of $\Lambda/\pi=0,91$, and it was found that the maximum achievable slenderness in SL-D1 was reduced to $\Lambda/\pi=0,93$ because of the residual acceleration.

To check the isorotational instability. Three times the instability was excited at the level predicted by theory, and the liquid column did broke indeed. However, in the last trial the deformation was not as expected, and this is attributed to the effect of the residual acceleration. Shortage of time in SL-D1 prevented to carry out a last trial were this would have been elucidated. A specific experiment on this point is scheduled for TEXUS-23 in late 1989.

To check the vibrational response of the column. Forced axial oscillations were imposed and the response was qualitatively (number of nodes) and quantitatively (between $\pm 50\%$ in frequency) in agreement with theory. A thorough study of resonances and amplitude response is scheduled for SL-D2 in late 1991.

Although not set as an objective, the residual acceleration imposed by the carrier is accurately measured, and a value of $70 \pm 10 \mu g_0$ was found. For future experiments, accelerometers must be as close as possible to the test volume.

Data reduction procedures are described, estimations of expected uncertainty in experimental results and explanations for deviations of results beyond uncertainty margins are given.

As for the logistics, crewman support was essential to success because most of the initially allocated time was spent solving infancy problems. The need for automated logbook-keeping and image analysis shows up clearly.

Acknowledgement: This work is being sponsored by the Spanish CICYT under Project No. ESP-88-0359.

6. REFERENCES

- Martínez, I. & Eyer, A., 1986, "Liquid Bridge Analysis of Silicon Crystal Growth Experiments under Microgravity", *J. Crystal Growth*, Vol. 75, pp. 535-544.
- Martínez, I., Haynes, J.M. & Langbein, D., 1987, "Fluid Statics and Capillarity", in *Fluid Sciences and Materials Sciences in Space, a European Perspective*, Springer-Verlag, pp. 53-81.
- Martínez, I., 1987, "Stability of Liquid Bridges. Results of SL-D1 Experiment", *Acta Astronautica*, Vol. 8, pp. 449-453.41.
- Meseguer, J. & Sanz, A., 1985, "Numerical and Experimental Study of the Dynamics of Axisymmetric Slender Liquid Bridges", *J. Fluid Mech.*, Vol. 153, pp. 83-101.
- Da Riva, I. & Manzano, D.R., 1981, "Impulsive Motions of the Floating Zone", *Physico Chemical Hydrodynamics 2*, pp. 165-176
- Sanz, A. & Perales, J.M., 1989, "Liquid Bridge Formation", *Appl. Microgravity Technology*, in press.
- Carlsaw, H.S., 1950, "Introduction to the Theory of Fourier Series and Integrals", Dover Publ. Inc., New York, pp. 269-271.
- Meseguer, J., 1988, "Axisymmetric Long Liquid Bridges in a Time-Dependent Microgravity Field", *Applied Microgravity Technology*, Vol. 1, pp. 136-141.
- Arbott, A.P., 1988, "Making Acceleration Data More Accessible and Useful to Microgravity Investigators", *Met. Trans. 19A*, pp. 2631-2637.
- Sanz, A. & López Díez, J., 1989, "Non-axisymmetric oscillations of Liquid Bridges", *J. Fluid Mech.* Vol. 205, pp. 503-521.